Food Chemistry: X 22 (2024) 101261

Contents lists available at ScienceDirect

Food Chemistry: X

journal homepage: www.sciencedirect.com/journal/food-chemistry-x

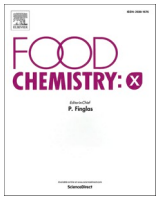

Characterization of antimicrobial multilayer film based on ethylcellulose-pectin incorporated with nanoemulsions of *trans*-cinnamaldehyde essential oil

Fatemeh Baghi [a,b], Adem Gharsallaoui [a], Emilie Dumas [a], Géraldine Agusti [a], Sami Ghnimi [a,b,*]

[a] Univ Lyon, Université Claude Bernard Lyon 1, LAGEPP UMR 5007, F-69622, Villeurbanne, France
[b] ISARA, 23 Rue Jean Baldassini, 69007 Lyon, France

ARTICLE INFO

Keywords:
Ethylcellulose
Pectin
Multilayer film
Nanoemulsion
Antimicrobial activity
Active packaging

ABSTRACT

In this study, polymer solution casting was utilized to fabricate a multilayer film with ethylcellulose (EC) as the outer layers and *trans*-cinnamaldehyde-loaded pectin as the inner layer. A significant increase in whiteness and UV–visible light blocking capability and a remarkable decrease in total color difference and yellowness of the films were seen via increasing the thickness of EC outer layers. Scanning electronic microscopy observation showed that the inner and outer layers had a smooth and uniform surfaces with clear boundary. The thicker film has better stretchability and strength, but is less flexible than thinner film. Glass transition temperature did not change remarkably with increasing thickness of EC outer layers, but thermal stability was slightly improved. FTIR-ATR spectra revealed the formation of hydrogen bonds between the two adjacent layers. The multilayer films exhibited excellent antimicrobial efficacy against Gram-positive and Gram-negative foodborne pathogens. The results suggested that this multilayer film has potential applications in active food packaging.

1. Introduction

The ubiquitous presence of microplastics in the environment constitutes a serious threat to human health and animal life. Consequently, the fight against plastic pollution has become a major societal concern. Plastic production has increased almost 230-fold since 1950, and nearly 40 % of the 400 million tons of plastic produced annually worldwide (as of 2016) is devoted to packaging, according to National Oceanic and Atmospheric Administration (NOAA). It is estimated that food packaging counted for approximately 45 % of non-biodegradable plastics (Tambawala et al., 2022). Given these alarming statistics, it is clear that biodegradable packaging is an urgent necessity.

The use of biopolymers in the manufacture of food packaging films has attracted much interest in recent years due to their biodegradability, non-toxicity, and renewable biosources. However, there is a need to improve the physical, mechanical, and barrier properties of biopolymer-based packaging films. Food spoilage is a major concern for both human health and the economic well-being of the food industry. To ensure public health, there is a need to provide safe products and ensure the shelf life of food during storage. In addition, consumers prefer natural, safe, and high-quality food products without synthetic preservatives. Therefore, there is an increasing need to develop natural and effective preservatives to meet this demand. Natural biomolecules derived from plants, such as those with antimicrobial and/or antioxidant activities can be used as preservatives in foods. Essential oils extracted from plants are considered ideal natural food preservatives and generally have GRAS (Generally Recognized as Safe) status (Falleh et al., 2020). Numerous studies have demonstrated the potential of essential oils to extend the shelf life of food products, allowing them to be used in packaging systems as active compounds that can be released over time to extend the shelf life of the packaged food. Active packaging is designed to extend the shelf life or improve the condition of the packaged food by modifying the environmental conditions during the preservation period (Soltani Firouz et al., 2021). This approach can be applied to the preservation of fresh foods and uses various strategies such as oxygen scavengers, carbon dioxide emitters/absorbers, ethylene scavengers, antimicrobial and antioxidant active packaging(Alves et al., 2023). Among these, antimicrobial packaging plays a central role in active food packaging, which aims to prevent or regulate microbial growth after food processing. The release of active compounds from active packaging is typically triggered by specific environmental factors or conditions, such as changes in temperature, humidity, pH or exposure to certain

* Corresponding author at: Univ Lyon, Université Claude Bernard Lyon 1, LAGEPP UMR 5007, F-69622, Villeurbanne, France.
E-mail address: sami.ghnimi@univ-lyon1.fr (S. Ghnimi).

https://doi.org/10.1016/j.fochx.2024.101261
Received 7 August 2023; Received in revised form 26 February 2024; Accepted 27 February 2024
Available online 29 February 2024

gases (Soltani Firouz et al., 2021). Many fresh products have a high moisture content, which causes the release of active compounds from the packaging into the fresh food products (Zhang et al., 2023). The pectin-based film incorporated with the essential oils of *Thymus capitatus* and *Cinnamomum verum* showed antimicrobial and antioxidant activity (Khachani et al., 2024). Successful shelf-life extension of fresh-cut carrots with a blend of four essential oils (EOs) encapsulated in a pectin film was reported (Ben-Fadhel et al., 2020). Extended shelf-life of chicken fillet to 12 days and improved sensory quality, water retention and textural properties; reduced microbial, yeast and mold growth were obtained from pectin film containing curcumin and cinnamon essential oil (Abdou et al., 2018).

Multilayer active packaging has been developed to achieve desirable physical, mechanical, and barrier properties, which are essential for increasing the shelf life of food products. Multilayer films provide higher barrier properties, better mechanical properties, or heat sealability compared to monolayer films. This type of packaging film has also been proposed to control the release of active compounds from the active layer toward the packaged food (Vieira et al., 2022). Multilayer active films are designed with three layers: the first is the outer barrier layer, which prevents the loss of active substances to the environment; the second is the matrix layer, which contains the active compounds that will be released during storage; and the third is the control layer, which is in contact with food and controls the rate of active compound release. It is important to consider various parameters when designing a multilayer active film package suitable for a specific food product, including thickness, chemical composition, and diffusivity of the control layer (Sharma et al., 2020).

In previous studies, we have optimized the formulation of the *trans*-cinnamaldehyde (TCN) nanoemulsions and improved the pectin film properties (Baghi et al., 2023). In the present study, the effect of the thickness of the outer ethylcellulose layers on the antimicrobial, mechanical, microstructural, optical, and thermal properties of the active food packaging films was investigated.

2. Materials and methods

2.1. Materials

The ethylcellulose powder used in this study, with a 48.0–49.5 % (w/w) ethoxyl basis, was procured from Sigma Aldrich (Merck, Germany). Trans-cinnamaldehyde with a purity of 99 % was obtained from Sigma-Aldrich (St Quentin Fallavier, France), while granular soybean lecithin was purchased from Acros Organics (Germany). Low methoxyl pectin (LMP) with a degree ranging from 22 % to 28 % and acetylation degree from 20 % to 23 %, and a carbohydrate content of 81.21 %, was procured from Cargill (Baupte, France). Glycerol, used as a plasticizer, was purchased from PanReac AppliChem (ITW reagents, USA).

2.2. Preparation of nanoemulsions (NE)

To prepare the nanoemulsions (NE), 10 % (w/w) of TCN was first dispersed in distilled water by emulsifying 2 % (w/w) of soybean lecithin using a high-speed homogenizer (Polytronpt 2500 E, Kinematic, Swiss) for 6 min under 15000 rpm to form coarse emulsions. Subsequently, the coarse emulsions were passed through a microfluidizer (Microfluidizer LM20, Microfluidics Corp, Newton, MA, USA) twice at a pressure of 500 bar and once at a pressure of 1000 bar to obtain the nanoemulsions. To verify the size distribution and stability of the nanoemulsion, the size distribution and zeta potential were measured.

2.3. Preparation of antimicrobial multilayer films

2.3.1. Preparation of the film-forming solution

6 % (*w/w*) ethylcellulose (EC) was solubilized in absolute ethanol with 1.5 % (*w/w*) glycerol and 1.5 % (*w/w*) corn oil as the plasticizer, using a magnetic stirrer at room temperature for 4 h to prepare the film-forming solution of EC. The film-forming solution of pectin was prepared by solubilizing 9 % (w/w) pectin and 2 % (w/w) glycerol in distilled water, using a magnetic stirrer at room temperature for 4 h. Next, to prepare the active film-forming solution (PNE), the pectin solution was mixed with the nanoemulsion (NE) in a 3:1 (*w/w*) ratio, with continuous stirring at room temperature (23 ± 1 °C) for around 1 h. The selection of these relevant ratios was based on preliminary optimization tests.

2.3.2. Fabrication of multilayer active films

The mono and multilayer films were prepared by using an electrically driven film applicator device (Unicoater 409, ERICHZEN, Germany) and a four-way film applicator with fixed gap heights (Model 360, ERICHZEN, Germany) with the possibility of making different wet layer thicknesses (the layer thickness before drying). All films were made on the glass plates by casting the film-forming solution and were dried in an oven (UNB 400, Memmert, Germany) at the temperature of 60 °C. The monolayer films (EC 1 with a wet thickness of 500 μm, EC2 with a wet thickness of 1000 μm and PNE with a wet thickness of 1000 μm) were prepared by spreading the film-forming solution to the desired wet layer thickness. The multilayer films (M1 and M2) were prepared layer by layer in which the first layer of (EC1 or EC2) was spread on the glass plate and completely dried, then the second layer (PNE) was added and dried. Finally, the third layer of EC was spread out on the two-dried layers of the film. A design of two different thicknesses of the EC layers (EC1 or EC2) was investigated in this study. A representative scheme of the multi-layer films (M1 and 2) is shown in Fig. 1.

2.4. Characterization of the nanoemulsions

2.4.1. Size distribution

A dynamic light scattering (DLS) using a Zetasizer Nano-ZS90 (Malvern Instruments Ltd, Worcestershire, UK) at a fixed angle of 90° was used to determine the droplet size and polydispersity index (PDI) of nanoemulsions. Nanoemulsions were diluted by homogenizing 1 ml of nanoemulsion to 10 ml of distilled water to eliminate multiple scattering effects. After 90 s of equilibrium, the measurement was performed. The measurements were repeated in triplicate and the average droplet size and average PDI were calculated.

2.4.2. Zeta potential (ς)

Zeta potential of nanoemulsions particles was measured with Zetasizer Nano-ZS90 (Malvern Instruments Ltd, Worcestershire, UK) using disposable cuvettes for electrophoretic mobility measurement. The samples were diluted by homogenizing 1 ml of nanoemulsion in 10 ml of distilled water. Zeta potential was measured in triplicate and the mean value was calculated.

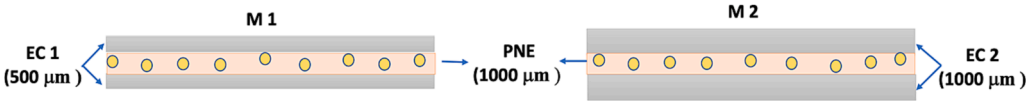

Fig. 1. The design of the M 1 and M 2 multi-layer films.

2.5. Films characterization

2.5.1. Film thickness

The thickness of dried film samples was determined using an electronic micrometer (Walmart 0–25 mm, 0.001 mm). Measurements were performed at least five different points of each film surface to calculate the average value.

2.5.2. Optical properties

The surface color (L, a, and b) of the different films was evaluated by using a colorimeter (Spectrophotometer CM-2300d, Konica Minolta, Japan). A standard white plate (L* = 92.07, a* = 1.12, b* = −1.48) was used as the control. The L* value describes the lightness (0 = black to 100 = white). The a* value describes the amount of redness (positive) or greenness (negative) present in the sample. The b* value describes the amount of yellowness (positive) or blueness (negative) present in the sample. At least five points from each sample were selected to measure the colorimetric properties of the films. The total color differences (ΔE), whiteness (WI), and yellowness (YI) indexes were calculated as follows:

$$\Delta E = \sqrt{(L^* - L)^2 + (a^* - a)^2 + (b^* - b)^2} \quad (2)$$

$$WI = 100 - \sqrt{(100 - L)^2 + a^2 + b^2} \quad (3)$$

$$YI = (142.86xb)/L \quad (4)$$

where L*, a* and b* are the color parameter values of the standard plate and L, a, and b are the color parameter values of the film samples.

The films were cut into a rectangular strip shape (9 mm × 40 mm) and the light transmission of each film was performed using an UV-3100pc spectrophotometer (VMR, USA) at wavelengths ranging from 200 to 800 nm (near UV and visible regions).

2.5.3. Mechanical properties

Mechanical properties were determined according to the ASTM D882 standard method using the EZ Test EZ-X series tensile analyzer (Shimadzu Corporation, Kyoto, Japan) with a 500 N load cell connected with Trapezium X (Shimadzu autograph software). The film samples were cut into 15 mm × 100 mm square shape. They were conditioned at RH = 55 % for one week, then mounted in two grips with the specimen's gauge length of 50 mm, and testing was performed at a crosshead speed of 50 mm/min. Tensile strength (TS), elongation at break (%EAB) and Young's modulus (YM) were calculated as follows:

$$TS = \frac{F_m}{x^* w} \quad (5)$$

$$EAB(\%) = \frac{\Delta L}{L_0} \times 100 \quad (6)$$

$$YM = \frac{TS}{\Delta L / L_0} \quad (7)$$

where F_m (N) is the maximum tensile force; x and w (m) are the thickness and width of the films, respectively; ΔL is the increase in the length before breakage; and L_0 is the initial length of the film.

2.5.4. Thermal properties

Differential scanning calorimetry (DSC) experiments were carried out in a DSC Q2000 device (TA instruments, New Castle, USA). Samples of approximately 5 mg were placed into aluminum pans, sealed and scanned over the range of −20–220 °C with a heating rate of 10 °C/min. The chamber was purged with nitrogen gas at a flow rate of 50 cm^3/min. The glass transition temperature (Tg) of the films was determined by analyzing the DSC thermograms using TA Universal Analysis Software.

The thermal stability of the film samples was tested with thermogravimetric analysis (TGA) (TG 209 Netzsch, Germany). Alumina crucibles were filled with accurately weighted samples of about 10 mg. The temperature program ranged from 20 °C to 600 °C at a heating rate of 10 °C/min. All experiments were conducted under a nitrogen atmosphere. The weight loss was recorded as a function of temperature and time to obtain TGA data.

2.5.5. Attenuated total reflectance-Fourier-transform infrared (ATR-FTIR) spectroscopy

The film samples were analyzed using an FTIR spectrophotometer coupled with ATR (FTIR: Nicolet iS50, Waltham, USA). All FTIR spectra were carried out at a resolution of 4 cm^{-1} with 64 scans in the spectral range of 4000–400 cm^{-1}.

2.5.6. Scanning electron microscopy

Scanning Electron Microscopy (SEM) was performed using an FEI Quanta 250 microscope (Eindhoven, Netherland) at the "Centre Technologique des Microstructures" (CTμ) at the University of Claude Bernard Lyon 1 (Villeurbanne, France). Film samples were deposited on a flat steel holder. The samples were coated under vacuum by cathodic sputter before conducting microscopy analysis.

2.6. Antimicrobial activity

The disk diffusion method was applied to investigate the antibacterial effect of films against two Gram-positive bacteria, *Listeria innocua* (DSM20649) and *Brochothrix thermosphacta* (DSM20171) and two Gram-negative bacteria *Escherichia coli* (DSM613) and *Salmonella Typhimurium* (DSM11320). The strains were provided by DSMZ-German Collection of microorganisms. Strains were stored at −20 °C in Tryptone Soy Broth (TSB) (Biokar diagnostics, Beauvais, France) with 15 % (v/v) of glycerol. One milliliter of the stock culture was transferred to 9 ml of TSB and incubated for 7 h at 37 ± 1 °C (*E. coli*, *L. innocua*, and *S. Typhimurium*) or at 30 ± 1 °C (*B. thermosphacta*). One milliliter of this pre-culture was transferred in 9 ml of TSB and incubated overnight at 37 ± 1 °C or 30 °C. Finally, one milliliter of this culture was transferred to 9 ml of TSB and incubated for 5 h at 37 ± 1 °C or 30 ± 1 °C. The cultures of bacteria were then diluted into TSB to obtain approximately 10^6 CFU (Colony Forming Units) /mL. Each culture was then used to inoculate at 5 % the Petri dishes containing Tryptone Soy Agar (TSA) (Biokar diagnostics, Beauvais, France). The film samples were cut aseptically in a disc shape with a diameter of 16 mm via a hole puncher. The disc of films was placed on the surface of TSA plates and then they were incubated for 24 h at the temperature of 37 ± 1 °C for *E. coli*, *L. innocua*, and *S. Typhimurium,* and 30 ± 1 °C for *B. thermosphacta*. The diameter of inhibition zones around the film discs was measured by using a digital vernier caliper (IHM). The experiments were made in triplicate for each film.

2.7. Statistical analysis

All tests were performed in at least triplicate. Data were presented as means ± standard deviation for different samples. One-way analysis of variance (ANOVA) was used, followed by Fisher's test (F) to compare the means. The difference was considered significant at $p < 0.05$.

3. Results and discussions

3.1. Particle size and zeta potential of nanoemulsions

The average size of the nanoparticles of the emulsion was 106 ± 2 nm with the polydispersity index (PDI) around 0.24 ± 0.04. According to ISO standards ISO 22412:2017 and ISO 22412:2017, the emulsion had a polydisperse distribution of particles. The average zeta potential

was – 57 ± 2 mV, indicating good emulsion stability due to the high zeta potential values. This is mainly due to the high degree of electrostatic repulsion that causes resistance to aggregation for any absolute zeta potential above 30 mV (Duffy et al., 2012). The negative charge and the small mean size of nanoemulsion particles are due to use the of lecithin which is a negatively charged phospholipid with good emulsifying properties and high affinity with essential oil components (Y. Yang et al., 2021).

3.2. Optical properties of the films

Color and transparency are essential parameters in food packaging, which are of key relevance that could influence the decision of consumers. The film transparency affects its application and represents the barrier property of light. The light transmission refers to the ability of light to pass through the film packaging, which has some implications such as product visibility and oxidative deterioration prevention. The higher the light transmission value, the more transparent it is and the less light protection it provides. Light can promote the oxidation of food, leading to a decline in nutritional value and a change in color, and the formation of off-flavors. In this study, we investigated the effect of the EC film thickness on its color and optical properties. The UV–vis spectra of the different films are shown in Fig. 2 and the thickness and optical properties are summarized in Table 1.

From Fig. 2, we can see that PNE film showed the lowest light transmission of 5.65 ± 0.24 % due to the addition of the nanoemulsion of *trans*-cinnamaldehyde. The monolayer films EC1 and EC2 had light transmission values of 69.97 ± 3.64 % and 60.82 ± 2.85 % indicating their transparency. While EC2 had less transparency because of its higher thickness. The same trend was observed for multilayer films. M1 has a light transmission of 41.9 ± 1.89 %, whereas M2 has a light transmission of 31.24 ± 3.29 %, due to its greater thickness. Indeed, increasing thickness leads to a reduction in light transmission and transparency. Surface pores strongly scatter visible light (Nogi et al., 2009). As thicker layers need more time to dry, surface pores are larger, so increasing thickness reduces transparency.

For the EC monolayer films, there is no significant difference between the color parameters, except for the lightness (L) which is slightly higher for the thinnest film EC1. This indicates that increasing the thickness of the EC monolayer film decreases the lightness of the film. However, all color parameters listed in Table 1 changed for multilayer films M1 and M2. Lightness (L) and whiteness index (WI) were improved with a thicker layer of EC2. The other parameters such as redness (a) and yellowness (b) as well as total color difference (ΔE) and yellowness index (YI) decreased from the thinnest film M1 to the thickest film M2. This is because the thicker EC layer (EC2) had altered most of the color properties of PNE layer, which is yellowish because it contains the yellowish TCN nanoemulsion. A similar result was obtained by Hosseini et al (2016) who demonstrated that a multilayer film composed of polylactic acid (PLA) and fish gelatin shows a reduction in the ΔE value of the multilayer film compared to the PLA monolayer film.

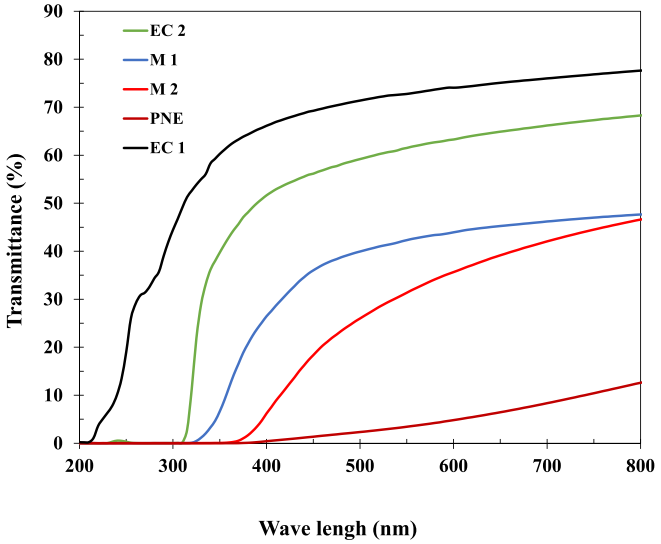

Fig. 2. UV–vis transmittance spectra of different films;

3.4. Mechanical properties

The mechanical properties of packaging films are important parameters for maintaining their integrity and tolerating external stresses during transport and their life cycle. The mechanical properties of the films are shown in Table 1. The PNE film had the highest EAB (8.12 %) compared with the other monolayer films but had the lowest YM (95.24 MPa). For the EC monolayer films of different thicknesses, the thickness had a significant effect on the improvement in maximum force tolerated before breaking (Fm). EC1 withstood a force of 4.12 ± 0.10 N before breaking, while EC2 withstood a force of 10.19 ± 0.61 N. However, tensile strength (TS) did not change significantly by changing the thickness for EC monolayer films. EAB also increased from 5.39 ± 0.61 % to 8.04 ± 0.29 % between EC1 and EC2. However, the YM decreased from 353.20 ± 9.49 to 276.29 ± 9.11 MPa for EC1 and EC2, respectively. This result is in line with the work of Wang et al. (2000), who reported that the YM is thickness-dependent; a thinner film has a higher YM.

The same effect of thickness was observed for M1 and M2 multilayer films. M2, a thicker multilayer film, showed the highest Fm of 17.06 ± 1.40 N, the highest force tolerated compared to all mono and multilayer film samples. TS and EAB also increased with thickness by around 43.91 % and 16.31 %, respectively. The YM of M2 was lower than that of M1. This could be attributed to the effect of the two layers of EC2 with a thickness of about 68 ± 3 μm causing less elasticity. A low YM (also known as the elastic modulus) results in a ductile film and a high YM results in a brittle film. Consequently, a thicker EC layer relatively improves the mechanical properties of multilayer films. The thicker multilayer film (M2) showed more stretchability and resistance, but it is less flexible compared to the thinner M1 film. There were significant differences in the values of the four parameters measured (Fm, TS, EAB, and YM) between the M1 and M2 multilayer films, indicating the effect of thickness on the mechanical properties of the multilayer packaging film.

3.5. Microstructure analysis by SEM

SEM was used to assess the surface morphology and cross-sectional structure of the films as shown in Fig. 3. The different structures have an impact on the properties of the films. Surface images of the two EC film monolayers (EC1 and EC2) show a rather smooth, uniform surface and different pores on the surface. SEM cross-section images of EC1 and EC2 revealed the amorphous structure of EC films. A similar study also revealed the same morphology for EC films (Mahnaj et al., 2013). The PNE film showed a dense, firm cross-sectional structure and a smooth surface morphology with a homogeneous structure. However, a few pores of all sizes were apparent in the PNE cross-section and surface images, but fewer than the EC films. Similar to these results, Espitia et al. (2014) revealed a rather smooth morphology with the presence of a few pits in a pectin film incorporated with apple skin polyphenols and thyme essential oils.

The surface morphology of the multilayer films was similar to that of the monolayer EC film. Heterogeneous pores were observed on the surface of all films. The porosity can be explained by the drying process, which results in the formation of pores on the films. The presence of the pores could be due to the rapid evaporation rate of the solvent during the drying process. Indeed, polymer segments become entangled with each

Table 1
Thickness, optical and mechanical properties of monolayer and multilayer films.

Film samples	Thickness (μm)	%T at 600 nm	L	A	b	ΔE	WI	YI	Fm (N)	TS (MPa)	EAB (%)	YM (MPa)
PNE	66 ± 1^{d}	5.65 ± 0.24 ^{e}	85.78 ± 0.26^{d}	−4.15 ± 0.21^{d}	33.37 ± 1.9^{a}	35.80 ± 1.92^{a}	−1236 ± 135^{c}	55.58 ± 3.34^{a}	6.27 ± 0.12^{c}	6.56 ± 0.03^{b}	8.12 ± 0.51^{c}	95.24 ± 12.20^{c}
EC1	30 ± 2^{e}	69.97 ± 3.64 ^{a}	90.75 ± 0.05^{a}	0.99 ± 0.04 ^{a}	−1.13 ± 0.04^{d}	1.36 ± 0.04^{d}	12.29 ± 1^{a}	−1.77 ± 0.07^{d}	4.12 ± 0.10 ^{d}	9.82 ± 0.24 ^{a}	5.39 ± 0.61 ^{d}	353.20 ± 9.49 ^{a}
EC2	68 ± 3^{c}	60.82 ± 2.85^{b}	89.63 ± 0.07^{b}	1.02 ± 0.02^{a}	−0.63 ± 0.02^{d}	2.57 ± 0.06^{d}	−8.85 ± 1^{a}	−1 ± 0.03^{d}	10.19 ± 0.61^{b}	9.49 ± 0.61 ^{a}	8.04 ± 0.29^{c}	276.29 ± 9.11^{b}
M1	124 ± 2^{b}	41.9 ± 1.89^{c}	85.16 ± 0.19^{e}	−0.57 ± 0.01^{b}	16.31 ± 0.15^{b}	19.16 ± 0.20^{b}	−386.82 ± 10^{b}	27.37 ± 0.31^{b}	7.55 ± 0.32 ^{c}	4.19 ± 0.17^{c}	15.51 ± 1.20^{b}	86.48 ± 14.58 ^{d}
M2	198 ± 3^{a}	31.24 ± 3.29 ^{d}	87 ± 0.15^{c}	−0.98 ± 0.05^{c}	13.56 ± 0.71^{c}	16.01 ± 0.69^{c}	−254.28 ± 21^{b}	22.27 ± 1.18^{c}	17.06 ± 1.40 ^{a}	6.03 ± 0.41^{b}	18.04 ± 0.74 ^{a}	157.25 ± 2.65^{c}

The data represent the mean ± one standard deviation (n = 3). Means with the same letters are not significantly different P ≤ 0.05).

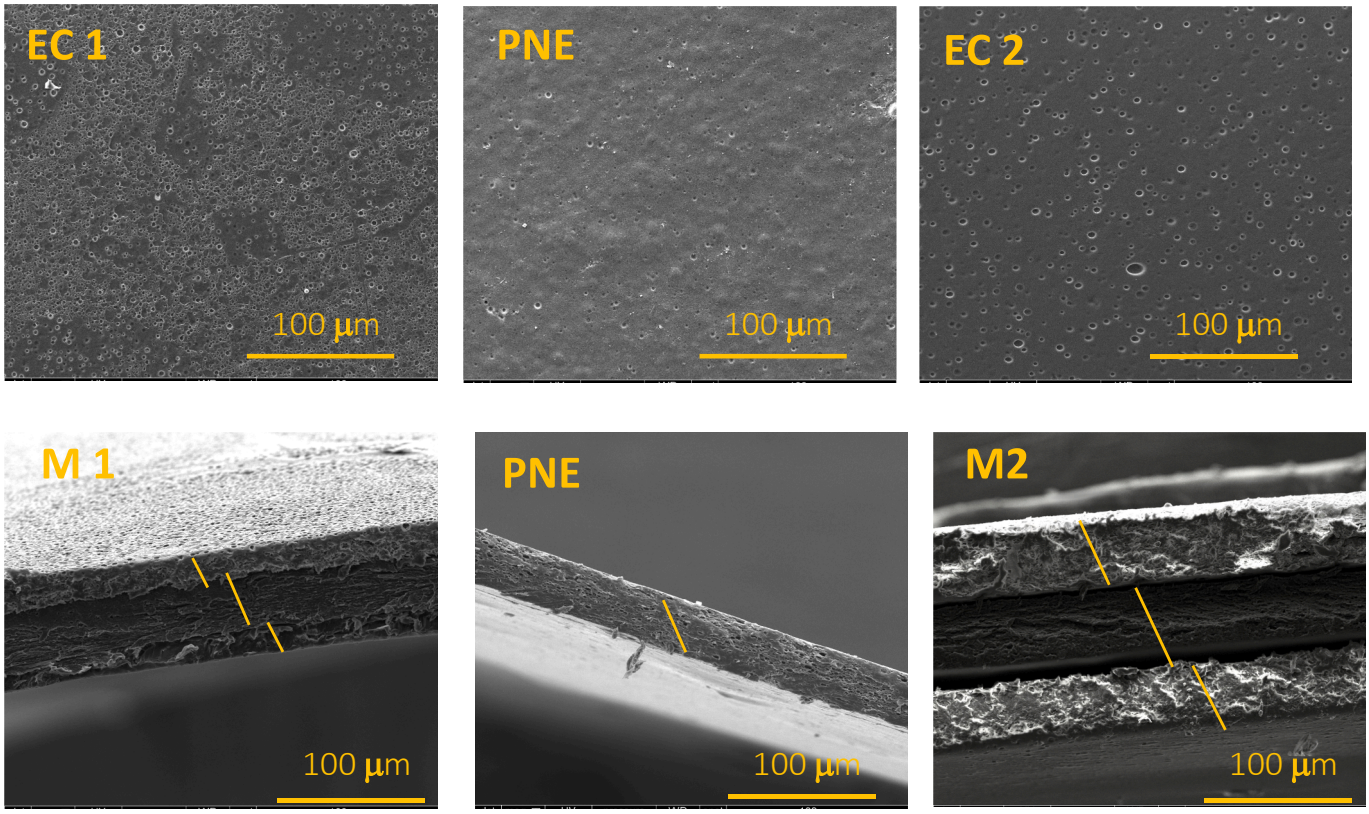

Fig. 3. Microscopic surface images of the films 400 x (first line); Microscopic cross-sectional image of films 400 x (second line).

other during drying due to the rapid evaporation of the solvent and, simultaneously, the polymer cannot form a continuous structure due to the short evaporation time. This increases the possibility of forming a porous network (Taylor et al., 2009).

As ethanol evaporation is faster for EC layers, more pores were observed. More pores were also observed on the surface of EC2 and M2 than on EC1 and M1. This is because the thicker EC layer takes longer to dry, resulting in the formation of more pores. It has been reported that chloroform evaporation caused a large number of microvoids and defects on the three-layer film derived from bovine gelatin (Martucci & Ruseckaite, 2010). In the case of multilayer films, the three layers are distinct. The boundary between the layers can be clearly observed. The middle layer (PNE) showed good adhesion to the inner and outer layers of the EC. The same interlayer behavior was reported by Wang et al. (2020) for a multilayer film of ethylcellulose and gelatin.

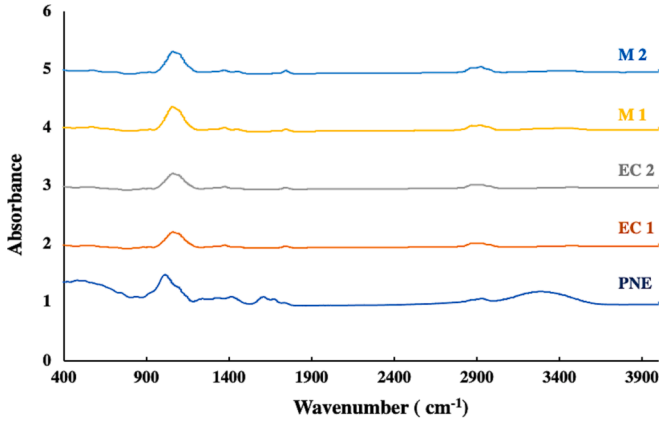

Fig. 4. ATR-FTIR of monolayer and multilayer films.

3.6. ATR-FTIR analysis

The chemical structure of the single and multilayer films was investigated by ATR-FTIR analysis, and the obtained spectra are shown in Fig. 4. The EC film showed a distinct peak at 3471 cm^{-1} corresponding to the stretching vibration of hydrogen-bonded - OH groups present in the glycerol added as a plasticizer (Hosseini et al., 2016). The peaks at 2919 and 2869 cm^{-1} attributed to –CH, and the following peaks at 1743, 1450, and 1370 cm^{-1} correspond to C═O, –CH2, and –CH3, respectively (Li et al., 2015). The broad distinct peak at 1059 cm^{-1} is due to the C— O- C stretch in the cyclic ether (Desai et al., 2006). The two last peaks at 919 and 879 cm^{-1} refer to –CH2 and –CH respectively and indicate the presence of epoxy groups (Zaitoon & Lim, 2020). The PNE film presented broad absorption regions between 3400 and 2500 cm^{-1} referring to the stretching vibration due to the –OH bonds among the pectin monomers (Singthong et al., 2004). The peak that appeared at 2927 cm^{-1} is assigned to the –CH stretching vibration of pectin's methylene and methyl groups (Roy & Rhim, 2021). The vibrational peaks around 1660, 1600, and 1400 cm^{-1} correspond, respectively, to asymmetric and symmetric vibrations of the carboxylate group (Manrique & Lajolo, 2002). The peak at 1013 cm^{-1} refers to the C— O- C stretching vibrations of the polymer chain structure. The peaks at 1237 cm^{-1} refer to –C—O– from ether linkage (Lal et al., 2021).

Multilayer films M1 and M2 show a peak quite similar to that of the EC monolayer film. However, the absorption band of –OH stretching was shifted from 3471 cm^{-1} for EC film to 3458 and 3460 cm^{-1} for M1 and M2, respectively. This indicates the formation of hydrogen bonds between two adjacent layers (Wang et al., 2017). A similar result was reported by Wang et al. (2020) who used sequential electrospinning to fabricate a multilayer film with ethyl cellulose nanofibers as the outer layers and curcumin-loaded gelatin nanofibers as the inner layer. Furthermore, in the case of the multilayer film, the intensity of the absorption peak at 1059 cm^{-1} changed. A higher intensity was observed for multilayer films compared to monolayer EC films, indicating that the C— O- C stretching vibrations are more abundant. This can be explained by the effect of the multilayer design, where three layers contain this bond. No shift in the peak position of the main groups, no peak disappearance, and no new peaks were observed in the spectra of M1 and M2 compared to the EC monolayer films. This result could be due to the penetration depth of the IR signal into the sample, which is typically

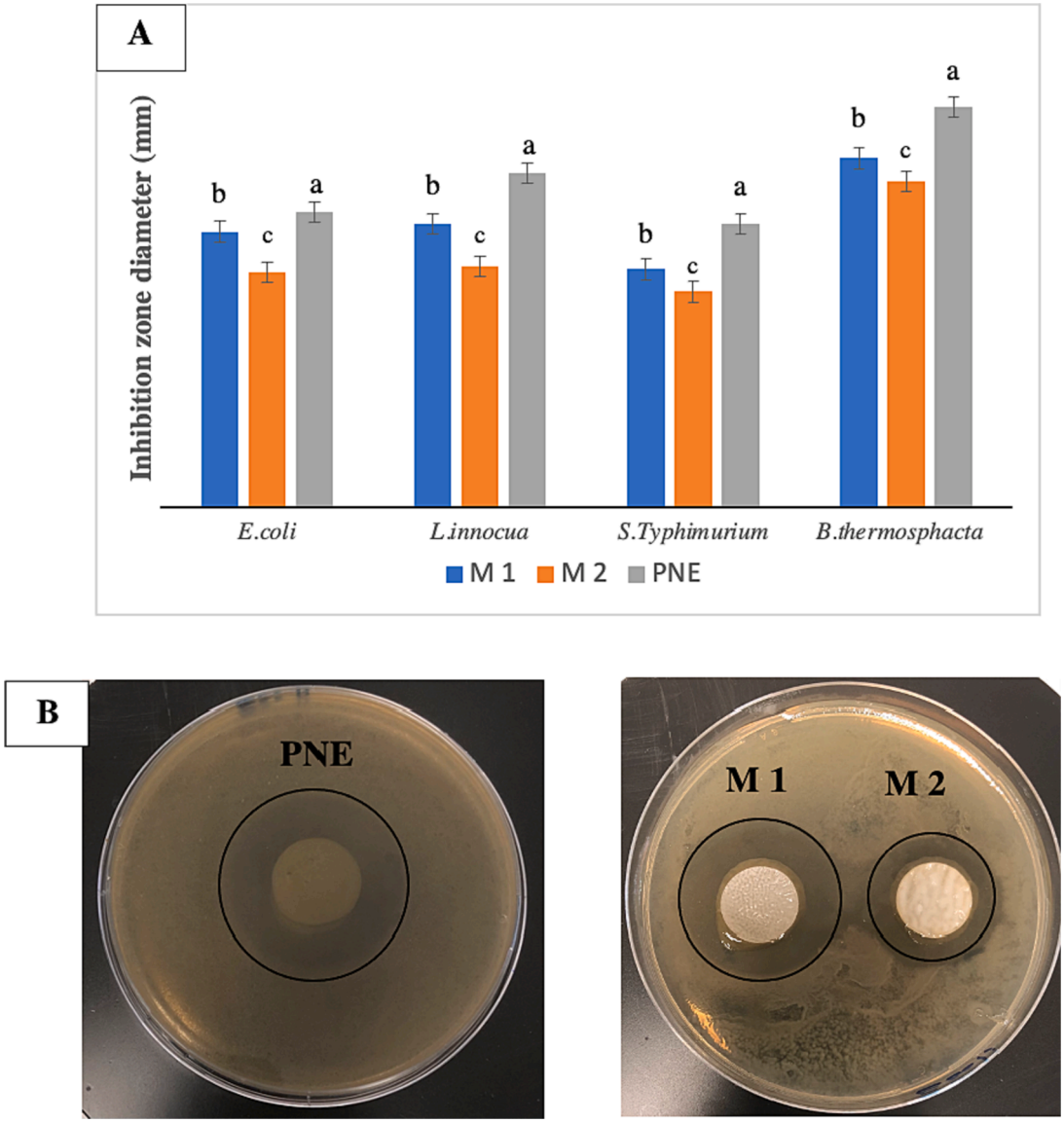

Fig. 5. (A) Antimicrobial effect of multilayer films (M1 and M2) and of monolayer film (PNE) containing TC on the four bacteria. (B) Images of the inhibition zone diameters of PNE, M1, and M2 on agar plates.

between 0.5 and 2 μm, whereas the thickness of the EC face in the multilayer structure is at least 30 μm (Hosseini et al., 2016).

3.7. Antimicrobial activity

The antimicrobial activity of the films against *E. coli, L. innocua*, *S. Typhimurium,* and *B. thermosphacta* is shown in Fig. 5. The EC film and the pectin film without TCN were used as controls to investigate the antimicrobial activity of pure ethylcellulose and pure pectin. No inhibition zones were observed for the controls, indicating that pure ethylcellulose and pure pectin do not have antimicrobial activity against the tested bacteria.

Zones of inhibitions were observed for the PNE film and the two multilayer films M1 and M2. The zones of inhibition were different according to the bacteria, in ascending order *B. thermosphacta* > *L. innocua* > *E. coli* > *S. Typhimurium*. The TCN antimicrobial agent was more effective against Gram-positive than Gram-negative bacteria. This is due to the more complex structure of Gram-negative bacteria, which possess a variety of polysaccharides, proteins, and lipid-based peptidoglycan. In fact, Gram-negative bacteria have an additional hydrophilic membrane containing lipopolysaccharide molecules. This prevents the penetration of hydrophobic compounds like essential oils. The Gram-positive bacteria lack this additional lipophobic outer membrane, which facilitates the penetration of hydrophobic compounds (Otoni et al., 2014). This is why the largest inhibition zones were observed for *B. thermosphacta* and *L. innocua as* Gram-positive bacteria compared to *E. coli* and *S. Typhimurium* as Gram-negative bacteria. These results are in line with the work of Hosseini et al., (2009) who used essential oils as antimicrobial agents in chitosan and pectin-based films.

The PNE film produced the largest zone of inhibitions compared with multilayer films for all four tested bacteria. This is explained by the presence of an extra layer of EC in the multilayer film samples, which slows down the release of TCN as an antimicrobial agent. In addition, the M1 multilayer film with a thinner EC layer showed a larger zone of inhibition than the M2 film with a thicker EC layer. This indicates the effect of thickness on the release rate of active compounds. The thicker EC layer results in a slower release rate and smaller zones of inhibition. The difference in inhibition zone diameter between multilayer films M1 and M2 was 2.22, 4.09, 3.94, and 2.18 mm for *B. thermosphacta*, *L. innocua, E. coli* and *S. Typhimurium*, respectively.

3.8. Thermal characterization

3.8.1. Differential scanning calorimetry (DSC)

Differential scanning calorimetry data analysis was applied to measure the glass transition temperature (Tg) of the films and assess the effect of the EC layer and its thickness on the Tg value (Table 2). Glass transition is a phenomenon of amorphous polymers in which polymers undergo a transition from a glassy to a rubbery state. It is an important characteristic of the behavior of the packaging films. It marks a region of dramatic changes in physical and mechanical properties. Under a temperature above Tg, due to a certain mobility, the films become soft and flexible like rubber. Tg is important to adjust extrusion parameters, such as temperature and plasticizer content. Thermal stability of the film formulations governs the process temperature for extrusion and compression molding. Tg has been considered the inflection point of the specific heat increment at the glass–rubber transition (Ahmad et al., 2021). The Tg of the pure pectin powder and pure ethylcellulose powder was measured to investigate the effect of plasticizers and essential oil on the Tg of films. Tg of pure pectin powder was 147 °C. The same result was reported in another study conducted by Ahmad et al., (2021) who obtained a Tg at 150.34 °C for pure pectin. EC is considered to be a highly or fully amorphous material.

The plasticizer enhances the free volume between the polymer chains, spacing them apart from each other, resulting in a decrease in Tg. In addition, essential oils act as a plasticizer that increases the mobility of polymer chains, caused by an increase in free volume between them (Qin et al., 2015). The Tg of the pectin-based film incorporated with the TCN nanoemulsion was determined at 54 °C. This significant decrease in Tg originates from the presence of glycerol and TCN as an essential oil in the composition of PNE film.

The same reduction was observed for Tg in the presence of essential oils in other studies. The neat ethylene vinyl alcohol copolymer (EVOH) had a Tg located at 55 °C. However, EVOH incorporated with different amounts of cinnamaldehyde showed Tg values, of up to 14 °C (Aragón-Gutiérrez et al., 2021).. The Tg of the EC film was determined at 99.5 °C for the same reason of the presence of glycerol and corn oil as plasticizers. The effect of corn oil on Tg of cassava starch was investigated by Madrigal et al (Madrigal et al., 2011), who found a decrease in the Tg. The multilayer films (M1 and M2) showed the relatively same Tg as PNE film, which is around 55 °C. This indicates that the thicker layer of EC does not have any effect on the Tg of multilayer films and the PNE interlayer affected the structure of the multilayer films, since Tg was reduced in comparison with neat EC film.

3.8.2. Thermogravimetric analysis (TGA)

TGA analysis helps to ensure the quality, performance and suitability of film packaging during processing and storage. This aids material selection, process optimization and quality assurance in the packaging industry. Understanding the thermal stability of film packaging is critical to selecting packaging materials that can withstand processing such as extrusion and storage conditions without significant degradation at elevated temperatures. TGA analysis was also performed to evaluate the effect of thickness and PNE interlayer on the thermal stability of EC/PNE/EC triple-layer films. In fact, the packaging film can potentially be exposed to extreme temperature variations during processing and storage such as heating, freezing or microwave irradiation. Therefore, the thermal decomposition behavior of the film samples was assessed between 20 and 600 °C. The weight loss curves of the films are shown in Fig. 6. In general, the initial weight loss comes from solvent vaporization, relatively high-water contents, and volatilization of volatile compounds that are present in samples. Subsequent stages correspond to the degradation of essential oils, plasticizers, and biopolymers. The highest rate of weight loss in the DTG curve considers the maximum degradation temperature T_m.

For the EC films (EC1 and EC2), two first steps of weight loss in the range of 20—300 °C were associated with evaporation loss and plasticizer weight loss. The main degradation of the EC film occurred at a

Table 2
Film weight loss (Δm) and glass transition of the film samples.

	Mass loss (Δm)					DSC
Film Samples	20 – 150 °C	150–300 °C	300—450 °C	450 – 600 °C	20 – 600 °C	Tg
PNE	7.42 %	47.16 %	13.61 %	4.82 %	73.05 %	54 °C
EC	3.78 %	14.87 %	78.21 %	1.68 %	98.57 %	99.5 °C
M1	6.77 %	39.10 %	34.55 %	3.13 %	83.33 %	55 °C
M2	5.30 %	31.62 %	48.65 %	2.55 %	88.12 %	55 °C
Thermal characterization	Solvent and volatile compounds evaporation	Plasticizers and pectindegradation	TC degradation	EC degradation	Total degradation	Transition from hard to brittle state

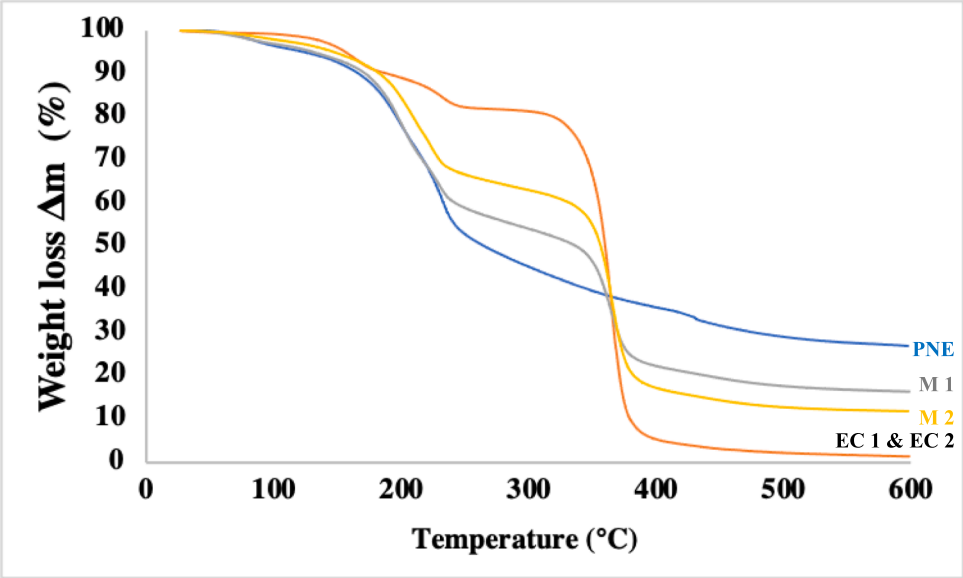

Fig. 6. TGA analysis of different films.

temperature of approximately 365 °C as $T_{m.}$ This temperature is higher than the T_m of the PNE film whose main degradation started at the temperature of about 232 °C.

This indicates that the thermal stability of the EC film is higher than that of the PNE film. Nevertheless, The EC film sample had a higher total mass loss. The EC films lost 98.57 % of their weight upon overheating from 20 to 600° C while this loss is 73.05 % for the PNE film sample. There was no obvious difference in mass change of EC1 and EC2 and their curves are superimposed in Fig. 5. The thermal behavior of multilayer films showed a behavior of combination of two component monolayers. The main mass loss of M1 and M2 occurred in two steps corresponding to the degradation of the PNE layer first followed by the degradation of the EC layers. Finally, the M1 and M2 multilayer films lost 83.33 % and 88.12 % of their mass, respectively. The mass loss of M2 was slightly higher due to the thicker EC layer, which undergoes more final degradation. These differences in thermal stability between multilayer samples come from the thicker layers of EC in the M2 thicker film, which translates into better thermal stability with increasing EC layer thickness for the multilayer films.

The thermal characterizations of film samples in different intervals are illustrated in Table 2. The mass loss in the first interval (20 – 150 °C) refers to the evaporation of water, ethanol, and the volatile part of TCN. The second one (150 – 300 °C) comes from plasticizers and pectin for the samples containing pectin. This result is consistent with the weight loss in pure pectin films at 110–250 °C reported by Ahmad et al. (2021). Hydrolysis or oxidation of *trans*-cinnamaldehyde occurred in this range. The degradation of TCN was obtained around 265—260 °C by (Hill et al., 2013).

Degradation of EC happened at the next interval (300 – 450 °C). This is in agreement with the result reported by (D. Yang et al., 2014), who observed that the degradation of pure EC film began at 290 °C. At the higher temperature interval (450 – 600° C), the degradation of the residual remnant occurred.

4. Conclusion

This study focuses on the design of an innovative plant-based multilayer antimicrobial film packaging for food products with the aim of extending their shelf-life in an environmentally friendly way. For this, TCN essential oil was used as an active component to prepare stable nanoemulsions. Subsequently, pectin films loaded with TCN nanoemulsions were fabricated and combined with two outer layers of EC with different thicknesses to produce a multilayer film EC/PNE/EC by using a layer-by-layer solvent casting method. The effect of the thickness of the outer EC layer was evaluated. Scanning electron microscopy revealed a good uniformity of the triple-layer films. DSC analysis revealed that PNE and EC materials are compatible showing only a reduction in glass transition temperature with PNE decomposition. At the same time, the results of this study indicate that increasing the thickness of the EC layer results in greater lightness and less yellowish and color differences and improved the UV–visible light blocking ability. In addition, the mechanical properties of the films are modified by changing the thickness of the ethylcellulose layer. In fact, increasing thickness of EC layer resulted in better stretchability and resistance, but less flexibility than the thinnest film. FTIR-ATR spectra revealed the formation of hydrogen bonds between two adjacent layers. The smallest zones of bacterial inhibition were observed for the thicker multilayer film, which indicates the effect of thickness on the release rate of TC from the PNE active layer. Based on the results of the present study, improving the outer layer of EC in multilayer films may have an effect on the biological properties of the films by slowing the release of TCN as a natural antimicrobial for food packaging. Consequently, the outcome revealed that thickness is a key factor in designing active multilayer films that impact the physical, mechanical, thermal, and antimicrobial properties of film packaging. These results showed that this biodegradable active film can be considered a potential substitute for non-biodegradable petroleum-based films for food packaging applications notably fresh foods due to hydrophobic layer of EC. Further studies are underway to assess the water vapor and oxygen barriers of triple-layer films.

CRediT authorship contribution statement

Fatemeh Baghi: Writing – original draft, Methodology, Investigation, Data curation. **Adem Gharsallaoui:** Writing – review & editing, Supervision, Methodology, Conceptualization. **Emilie Dumas:** Writing – review & editing, Supervision, Methodology, Conceptualization. **Géraldine Agusti:** Investigation, Data curation. **Sami Ghnimi:** Writing – review & editing, Supervision, Methodology, Funding acquisition, Conceptualization.

Declaration of competing interest

The authors declare that they have no known competing financial interests or personal relationships that could have appeared to influence the work reported in this paper.

Data availability

Data will be made available on request.

Acknowledgements

The authors would like to thank the TERRA ISARA foundation, for their financial support of this research project (grant number E-F0601-00).

References

Abdou, E. S., Galhoum, G. F., & Mohamed, E. N. (2018). Curcumin loaded nanoemulsions/pectin coatings for refrigerated chicken fillets. *Food Hydrocolloids, 83*, 445–453. https://doi.org/10.1016/j.foodhyd.2018.05.026

Ahmad, M. M., Chauhan, K., Naz, A., & Nayeem, M. (2021). Antimicrobial and antioxidant activity of impregnated pectin and alginate based bio composite packaging material for fresh produce safety. *The Pharma Innovation, 10*(8), 262–272. https://doi.org/10.22271/tpi.2021.v10.i8d.7176.

Alves, J., Gaspar, P. D., Lima, T. M., & Silva, P. D. (2023). What is the role of active packaging in the future of food sustainability? a systematic review. *Journal of the Science of Food and Agriculture, 103*(3), 1004–1020. https://doi.org/10.1002/jsfa.11880

Aragón-Gutiérrez, A., Heras-Mozos, R., Gallur, M., López, D., Gavara, R., & Hernández-Muñoz, P. (2021). Hot-melt-extruded active films prepared from EVOH/TRANS-cinnamaldehyde blends intended for food packaging applications. *Foods, 10*(7), Article 7. https://doi.org/10.3390/foods10071591

Baghi, F., Ghnimi, S., Dumas, E., Chihib, N.-E., & Gharsallaoui, A. (2023). Nanoemulsion-based multilayer films for ground beef preservation: Antimicrobial activity and physicochemical properties. *Molecules, 28*(11), Article 11. https://doi.org/10.3390/molecules28114274

Ben-Fadhel, Y., Maherani, B., Manus, J., Salmieri, S., & Lacroix, M. (2020). Physicochemical and microbiological characterization of pectin-based gelled emulsions coating applied on pre-cut carrots. *Food Hydrocolloids, 101*, Article 105573. https://doi.org/10.1016/j.foodhyd.2019.105573

Desai, J., Alexander, K., & Riga, A. (2006). Characterization of polymeric dispersions of dimenhydrinate in ethyl cellulose for controlled release. *International Journal of Pharmaceutics, 308*(1), 115–123. https://doi.org/10.1016/j.ijpharm.2005.10.034

Duffy, J., Larsson, M., & Hill, A. (2012). *Suspension stability; why particle size* (p. 20). Zeta Potential and Rheology are Important: Annual Transactions OF The Nordic Rheology Society.

Espitia, P. J. P., Avena-Bustillos, R. J., Du, W.-X., Teófilo, R. F., Soares, N. F. F., & McHugh, T. H. (2014). Optimal antimicrobial formulation and physical–mechanical properties of edible films based on açaí and pectin for food preservation. *Food Packaging and Shelf Life, 2*(1), 38–49. https://doi.org/10.1016/j.fpsl.2014.06.002

Falleh, H., Ben Jemaa, M., Saada, M., & Ksouri, R. (2020). Essential oils: A promising eco-friendly food preservative. *Food Chemistry, 330*, Article 127268. https://doi.org/10.1016/j.foodchem.2020.127268

Hill, L. E., Gomes, C., & Taylor, T. M. (2013). Characterization of beta-cyclodextrin inclusion complexes containing essential oils (trans-cinnamaldehyde, eugenol, cinnamon bark, and clove bud extracts) for antimicrobial delivery applications. *LWT - Food Science and Technology, 51*(1), 86–93. https://doi.org/10.1016/j.lwt.2012.11.011

Hosseini, M.h., Razavi, S.h., & Mousavi, M. A. (2009). Antimicrobial, physical and mechanical properties of chitosan-based films incorporated with thyme, clove and cinnamon essential oils. *Journal of Food Processing and Preservation, 33*(6), 727–743. https://doi.org/10.1111/j.1745-4549.2008.00307.x

Hosseini, S. F., Javidi, Z., & Rezaei, M. (2016). Efficient gas barrier properties of multi-layer films based on poly(lactic acid) and fish gelatin. *International Journal of Biological Macromolecules, 92*, 1205–1214. https://doi.org/10.1016/j.ijbiomac.2016.08.034

Hosseini, S. F., Rezaei, M., Zandi, M., & Farahmandghavi, F. (2016). Development of bioactive fish gelatin/chitosan nanoparticles composite films with antimicrobial properties. *Food Chemistry, 194*, 1266–1274. https://doi.org/10.1016/j.foodchem.2015.09.004

Khachani, R., El Galiou, O., Aitboulahsen, M., Bakrim, H., Arakrak, A., Laglaoui, A., & Hassani Zerrouk, M. (2024). Stability of antimicrobial, antioxidant, and functional properties of pectin-based film incorporated with Thymus capitatus and Cinnamomum verum essential oils. *Journal of Food Safety, 44*(1), e13097.

Lal, S., Kumar, V., & Arora, S. (2021). Eco-friendly synthesis of biodegradable and high strength ternary blend films of PVA/STARCH/PECTIN: Mechanical, thermal and biodegradation studies. *Polymers and Polymer Composites, 29*(9), 1505–1514. https://doi.org/10.1177/0967391120972881

Li, X., Jiang, F., Ni, X., Yan, W., Fang, Y., Corke, H., & Xiao, M. (2015). Preparation and characterization of konjac glucomannan and ethyl cellulose blend films. *Food Hydrocolloids, 44*, 229–236. https://doi.org/10.1016/j.foodhyd.2014.09.027

Madrigal, L., Sandoval, A. J., & Müller, A. J. (2011). Effects of corn oil on glass transition temperatures of cassava starch. *Carbohydrate Polymers, 85*(4), 875–884. https://doi.org/10.1016/j.carbpol.2011.04.013

Mahnaj, T., Ahmed, S. U., & Plakogiannis, F. M. (2013). Characterization of ethyl cellulose polymer. *Pharmaceutical Development and Technology, 18*(5), 982–989. https://doi.org/10.3109/10837450.2011.604781

Manrique, G. D., & Lajolo, F. M. (2002). FT-IR spectroscopy as a tool for measuring degree of methyl esterification in pectins isolated from ripening papaya fruit. *Postharvest Biology and Technology, 25*(1), 99–107. https://doi.org/10.1016/S0925-5214(01)00160-0

Martucci, J. F., & Ruseckaite, R. A. (2010). Biodegradable three-layer film derived from bovine gelatin. *Journal of Food Engineering, 99*(3), 377–383. https://doi.org/10.1016/j.jfoodeng.2010.02.023

Nogi, M., Iwamoto, S., Nakagaito, A. N., & Yano, H. (2009). Optically transparent nanofiber paper. *Advanced Materials, 21*(16), 1595–1598. https://doi.org/10.1002/adma.200803174

Otoni, C. G., de Moura, M. R., Aouada, F. A., Camilloto, G. P., Cruz, R. S., Lorevice, M. V., N. de Soares, F. F., & Mattoso, L. H. C. (2014). Antimicrobial and physical-mechanical properties of pectin/papaya puree/cinnamaldehyde nanoemulsion edible composite films. *Food Hydrocolloids, 41*, 188–194. https://doi.org/10.1016/j.foodhyd.2014.04.013

Qin, Y., Yang, J., & Xue, J. (2015). Characterization of antimicrobial poly(lactic acid)/poly(trimethylene carbonate) films with cinnamaldehyde. *Journal of Materials Science, 50*(3), 1150–1158. https://doi.org/10.1007/s10853-014-8671-8

Roy, S., & Rhim, J.-W. (2021). Preparation of pectin/agar-based functional films integrated with zinc sulfide nano petals for active packaging applications. *Colloids and Surfaces B: Biointerfaces, 207*, Article 111999. https://doi.org/10.1016/j.colsurfb.2021.111999

Sharma, R., Jafari, S. M., & Sharma, S. (2020). Antimicrobial bio-nanocomposites and their potential applications in food packaging. *Food Control, 112*, Article 107086. https://doi.org/10.1016/j.foodcont.2020.107086

Singthong, J., Cui, S. W., Ningsanond, S., & Douglas Goff, H. (2004). Structural characterization, degree of esterification and some gelling properties of krueo ma noy (Cissampelos pareira) pectin. *Carbohydrate Polymers, 58*(4), 391–400. https://doi.org/10.1016/j.carbpol.2004.07.018

Soltani Firouz, M., Mohi-Alden, K., & Omid, M. (2021). A critical review on intelligent and active packaging in the food industry: Research and development. *Food Research International, 141*, Article 110113. https://doi.org/10.1016/j.foodres.2021.110113

Tambawala, H., Batra, S., Shirapure, Y., & More, A. P. (2022). Curcumin- a bio-based precursor for smart and active food packaging systems: A review. *Journal of Polymers and the Environment, 30*(6), 2177–2208. https://doi.org/10.1007/s10924-022-02372-x

Taylor, J., Taylor, J. R. N., Belton, P. S., & Minnaar, A. (2009). Formation of kafirin microparticles by phase separation from an organic acid and their characterisation. *Journal of Cereal Science, 50*(1), 99–105. https://doi.org/10.1016/j.jcs.2009.03.005

Vieira, D. M., Andrade, M. A., Vilarinho, F., Silva, A. S., Rodrigues, P. V., Castro, M. C. R., & Machado, A. V. (2022). Mono and multilayer active films containing green tea to extend food shelf life. *Food Packaging and Shelf Life, 33*, Article 100918. https://doi.org/10.1016/j.fpsl.2022.100918

Wang, H., Hao, L., Wang, P., Chen, M., Jiang, S., & Jiang, S. (2017). Release kinetics and antibacterial activity of curcumin loaded zein fibers. *Food Hydrocolloids, 63*, 437–446. https://doi.org/10.1016/j.foodhyd.2016.09.028

Wang, J., Shi, F. G., Nieh, T., Zhao, B., Brongo, M., Qu, S., & Rosenmayer, T. (2000). Thickness dependence of elastic modulus and hardness of on-wafer low-k ultrathin polytetrafluoroethylene films. *Scripta Materialia - SCRIPTA MATER, 42*, 687–694. https://doi.org/10.1016/S1359-6462(99)00421-2

Wang, P., Li, Y., Zhang, C., Feng, F., & Zhang, H. (2020). Sequential electrospinning of multilayer ethylcellulose/gelatin/ethylcellulose nanofibrous film for sustained release of curcumin. *Food Chemistry, 308*, Article 125599. https://doi.org/10.1016/j.foodchem.2019.125599

Yang, D., Peng, X., Zhong, L., Cao, X., Chen, W., Zhang, X., Liu, S., & Sun, R. (2014). "Green" films from renewable resources: Properties of epoxidized soybean oil plasticized ethyl cellulose films. *Carbohydrate Polymers, 103*, 198–206. https://doi.org/10.1016/j.carbpol.2013.12.043

Yang, Y., Shi, Y., Cao, X., Liu, Q., Wang, H., & Kong, B. (2021). Preparation and functional properties of poly(vinyl alcohol)/ethyl cellulose/tea polyphenol electrospun nanofibrous films for active packaging material. *Food Control, 130*, Article 108331. https://doi.org/10.1016/j.foodcont.2021.108331

Zaitoon, A., & Lim, L.-T. (2020). Effect of poly(ethylene oxide) on the electrospinning behavior and characteristics of ethyl cellulose composite fibers. *Materialia, 10*, Article 100649. https://doi.org/10.1016/j.mtla.2020.100649

Zhang, W., Sani, M. A., Zhang, Z., McClements, D. J., & Jafari, S. M. (2023). High performance biopolymeric packaging films containing zinc oxide nanoparticles for fresh food preservation: A review. *International Journal of Biological Macromolecules, 230*, Article 123188. https://doi.org/10.1016/j.ijbiomac.2023.123188